Communication
Bioprocess Engineering and Supporting Technologies

Biotechnology and Bioengineering
DOI 10.1002/bit. 21323

Prediction of Mass Transfer Coefficients in Non-Newtonian Fermentation Media Using First-Principles Methods

Stefan Radl[1] *and Johannes G. Khinast*[2]

[1] *Institute RNS, Graz University of Technology*
Graz, Austria
[2] *Dept. of Chemical and Biochemical Engineering, Rutgers University, Piscataway, NJ 08845*

Received October 4, 2006; Accepted December 27, 2006

[2] Corresponding author: Johannes G. Khinast, currently Marie Curie Chair at the Institute for Process Engineering, Inffeldgasse 21 b, A-8010 Graz, khinast@tugraz.at, Tel. +43(0)316 873-7467, Fax. +43(0)316 873-7963

Abstract

Bubble flows in non-Newtonian fluids were analyzed using first-principles methods with the aim to compute and predict mass transfer coefficients in such fermentation media. The method we used is a Direct Numerical Simulation (DNS) of the reactive multiphase flow with deformable boundaries and interfaces. With this method we are able for the first time to calculate mass transfer coefficients in non-Newtonian liquids of different rheologies without any experimental data. In the current paper shear-thinning fluids are considered. However, the results provide the basis for further investigations, such as the study of viscoelastic fluids.

Keywords: numerical simulation, bubbles, non-Newtonian liquids, mass transfer

1 Introduction

Scale-up of bioreactors for the production of biopharmaceuticals, such as recombinant proteins, anti-infectives or vaccines, is known to be a challenging problem, due to a lack of general scaling laws for complex non-Newtonian media. The rheology of such fluids often exhibits strongly non-Newtonian behavior (Curtis, 1993; Doran, 1999; Kieran et al., 1997; Leduy et al., 1974; Rodriguez-Monroy et al., 1999, 2000; Sánchez et al., 2002). Furthermore, mass-transfer rates, which are needed for the prediction of oxygen supply, are not known a priori, since no general mass-transfer correlation exists for non-Newtonian fluids. Similar observations can be made for the properties needed to precisely predict transport of metabolites, nutrients or CO_2.

Most data on non-Newtonian liquids are derived from experimental studies, which are usually interpreted with simple theoretical models (Doran, 1999; Jin et al., 2005; Kawase and Hashimoto, 1996; Kieran et al., 1997; Li et al., 2004; Sánchez et al., 2002). However, so far there have been no reports on the prediction of mass transfer coefficients in non-Newtonian fluids based on first-principles methods. Thus, it is the aim of this contribution to present a new Direct Numerical Simulation (DNS) method that allows us to investigate in detail the micro-effects in non-Newtonian fluids, including the computation of mass transfer coefficients.

In addition to mass transfer and transport coefficients, knowledge of shear rates and the resulting stress distribution in aerated non-Newtonian liquids are important to determine whether a bioreactor is suitable to handle shear-sensitive biosystems (Al-Masry, 1999). Damage to fragile microorganisms, biofilms and immobilized biocatalysts due to high shear rates have been reported (Duddridge et al., 1982; Gjaltema et al., 1995, 1997; Kieran, 1993; Lau and Liu, 1993; Leenen et al., 1996; Martins dos Santos et al., 1997). However, even sub-critical shear stresses found in the hydrodynamic environment of large-scale reactors may reduce cell productivity by impacting transcription, translation, secretion and other mechanisms (Choi et al., 2006). Clearly, a better understanding of the underlying micro-processes will have a positive effect on bioreactor technology (Kieran et al., 1997). For example, external circulating loop airlift (ECL-AL) bioreactors are increasingly used in the biochemical industry. However, the design equations are mostly based on simple macro-scale models using empirical correlation. As a consequence optimization strategies are restricted to a limited number of variables. Another example includes high-density cell systems, which are increasingly used and where oxygen and nutrient supply are critical parameters (Choi et al., 2006).

In order to perform realistic macro-scale simulations (equipment size) of a turbulent bio-reactive flow, models of the micro-scale effects are required to capture all scales of the process, including the smallest eddies, bubble-cell interactions and oxygen transport. Such micro-scale models need to be assumption-free, i.e., one needs to use first-principle tools, such as Direct Numerical Simulation (DNS) methods.
Using DNS it is now possible to fully resolve the interface of a bubble in all three dimensions and even to predict the interaction of many deformable bubbles (Tryggvason et al., 2001). The inclusion of species conservation, however, has been a persistent problem, because of the high Schmidt numbers that require a large number of grid points needed to resolve the concentration field. For the first time, Koynov et al. (2005) performed DNS of this challenging problem and provided detailed results on mass transfer and chemical reactions in fully deformable bubble swarms. Our contributing is to extend their method to non-Newtonian flows, such as the ones encountered in biotechnological applications.

2 Method

In our study reactive DNS of bubbly flows in non-Newtonian liquids have been performed in order to predict mass transfer coefficients without use of any correlations. The method is based on a fully resolved simulation of the fluid dynamics and the concentration field around a single bubble on a grid containing more than 3,000,000 nodes. A modified 2D front-tracking/front-capturing method based on a code developed by Tryggvason et al. (2001) is used to simulate the motion of deformable gas bubbles. A newly developed scheme has been employed for the solution of the species conservation equations.

Fluid dynamics

In order to obtain the velocity field around deformable bubbles, the linear momentum equations, as well as the mass conservation equation have to be solved. For multiphase flows various techniques exist. In our method, the front of the bubble is directly tracked, and the material properties (density and viscosity) can then be reconstructed on a fixed grid. The jump in the material properties and the interphase momentum exchange at the phase boundary are directly captured that way. Therefore, we do not need any additional modeling. The linear momentum equation and the species conservation equation are solved in the entire domain, treating the multiphase system as a single fluid with changing properties, while accounting for surface tension forces. The governing equations can then be written as:

$$\frac{\partial \rho \cdot \vec{u}}{\partial t} + (\vec{u} \cdot \nabla)\rho\vec{u} = -\nabla p + \rho \cdot \vec{f} + \nabla \cdot \left[\mu(\vec{x}) \cdot \left(\nabla \vec{u} + \nabla^T \vec{u}\right)\right] + \oint \sigma\kappa' \vec{n}' \cdot \delta^2 \cdot (\vec{x} - \vec{x}') \cdot ds' \tag{1}$$

$$\nabla \cdot \vec{u} = 0 \tag{2}$$

The two equations are solved simultaneously for the time step n+1 in the computational domain using a two-step method. In the first step (prediction step) the pressure gradient in the momentum equations is neglected, and an intermediate velocity field u* is generated:

$$\frac{\rho^{n+1} \cdot \vec{u}^* - \rho^n \cdot \vec{u}}{\Delta t} = -\left(\vec{u}^n \cdot \nabla_h\right)\rho^n \vec{u}^n + \nabla_h \cdot \left[\mu^n(\vec{x}) \cdot \left(\nabla_h \vec{u}^{n+1} + \nabla_h{}^T \vec{u}^{n+1}\right)\right] + \vec{F}_\sigma \tag{3}$$

In Equation 3 the subscript h denotes the numerical approximation of the spatial derivative. For this step a Crank-Nicholson scheme was used to solve the implicit equation. Thus, in contrast to the former code (Koynov et al., 2005), no stability criterion has to be satisfied and the code is significantly faster. In the second step the pressure gradient is added, resulting in a Poisson equation that is solved with an SOR algorithm.

Constitutive equation for the continuous phase

A power law model (Eq. 4) and a Carreau-Yasuda (Eq. 5) shear-thinning model have been implemented. Once the local shear rate has been calculated at each nodal point of the domain, the apparent viscosity can be reconstructed. For the presented simulations a power law model with a low shear rate cutoff was used, because of its frequent use. However, any other model on the basis of a generalized Newtonian fluid can be used in the simulation.

$$\mu(\vec{x}) = K \cdot \dot{\gamma}(\vec{x})^{n-1} \tag{4}$$

$$\frac{\mu(\vec{x}) - \mu_\infty}{\mu_0 - \mu_\infty} = \left[1 + \left(\lambda \cdot \dot{\gamma}(\vec{x})\right)^a\right]^{\frac{n_{CY}-1}{a}} \tag{5}$$

Species Conservation Equation

The equation describing the transport of species α can be written as:

$$\frac{\partial c_\alpha}{\partial t} + (\vec{u} \cdot \nabla)c_\alpha = D_\alpha \cdot \nabla^2 c_\alpha + \sum_j \nu_{\alpha,j} \cdot r_j \tag{6}$$

For the mass transfer simulations the reaction rates r_j were set to zero. The solution of this partial differential equation (PDE) with direct discretization typically leads to inaccurate results because of the numerical diffusion introduced by the discretization of the convection term. In our simulation a novel semi-Lagrangian (SL) advection scheme was used that was initially developed for the application in atmospheric modeling (Staniforth and Côté, 1991). Since the Pèclet number of the problems is high (1,000 – 10,000 for the flow of air bubbles in an aqueous medium), the advection term is dominating the diffusion term. Therefore, the use of an accurate advection scheme producing no or an insignificant amount of numerical diffusion is critical. This was realized by the use of an operator splitting – SL – scheme that first advects the concentration directly from the departure point to the current grid point. Then, the algorithm carries out the diffusion and reaction step (Radl, Diploma Thesis, Graz University of Technology, 2006).

3 Results and Discussion

Enhancement of Numerical Algorithms

The implemented Crank-Nicholson scheme enabled us to reduce the computational time at low Re-numbers by about 90% due to the increased time-step size. Furthermore, it improved the stability of the non-Newtonian fluid simulations, enabling us to run simulations with a low power law index (strongly shear-thinning fluids). The SL-Advection scheme proved to result in low numerical diffusion. Thus, we are able to fully resolve the concentration boundary layer close to the bubble interface, even at the bubble roof. The computational cost of this scheme (interpolation at the departure point) was mostly absorbed by an adaptive algorithm that skips points where the advection terms can be neglected.

Validation of the Models

To validate the Semi-Lagrangian advection scheme, different tests were conducted. One test was to compare the experimentally and theoretically predicted mass-transfer rates in Newtonian fluids. In Fig. 1 the Sherwood number was plotted against the Reynolds-number. The comparison of the available data with the simulation results demonstrates the accuracy of the model. It can be seen from Fig. 1 that the results match other data in the range of their applicability very well. The validation of the power-law fluid model was based on the comparison of drag coefficients (Radl, Diploma Thesis, Graz University of Technology, 2006) and showed good agreement with correlations taken from the literature (see for example Margaritis et al., 1999).

Mass Transfer Coefficients as a function of the flow index n

As reported by Bhavaraju et al. (1978), the mass transfer coefficient increases with increasing pseudo plasticity and decreasing flow index. This finding can be confirmed as shown in Fig. 2, which shows the Reynolds number as a function of the flow index n. As can be seen from our simulations, the increase in the mass transfer rate is more pronounced in the low-Reynolds-number regime Re = 1, compared to the case of Re = 5. However, in the case of a recirculation wake (Re = 18) and at low flow indices a significant impact on mass transfer coefficients can be observed. For this case, shear thinning effects cause an increase of the mass transfer rate of up to 20%. Low values of the Schmidt number (Sc = 50) weaken the influence of the shear thinning effects on the mass transfer at Re = 1. For low Schmidt numbers, diffusion dominates convective effects, which are influenced by the non-ideality of the fluid. In the case of higher Schmidt numbers (Sc = 400), the concentration boundary layer is thinner and therefore, is located in a region close to the bubble interface, where shear thinning effects lower the local viscosity and result in a higher velocity gradient.

In Figure 2 we have also included an analytical correlation valid for infinite Pèclet numbers and creeping flows, which was derived by Hirose and Moo-Young (1969). Furthermore, experimental data for creeping flows by Moo-Young et al. (1970) are shown. As can be seen from Figure 2, our data for developed flows and realistic Sc number agree well with this theoretical analysis and the experimental study. As expected, the agreement improves for lower Reynolds number and higher the Schmidt numbers.

Concentration fields around bubbles in non-Newtonian liquids

From our simulations it can be seen that the concentration fields around bubbles in non-Newtonian liquids have a longer tail than those in Newtonian fluids (see Fig. 3), which is due to the lower viscosity in the wake. However, close to the bubble no substantial difference can be detected for low to moderate Re-numbers. Thus, only the reduced local viscosity close to the bubble interface and the higher viscosity in the wake of the bubble in non-Newtonian liquids are responsible for the increase of the mass transfer rate as illustrated in Fig. 2.

Shear rate distribution around the bubbles

The velocity field $\vec{u}$ has been used to calculate the local shear rate distribution $\dot{\gamma}(x,y)$. The shear rate $\dot{\gamma}$ is calculated according to:

$$\dot{\gamma} = \sqrt{2 \cdot D : D} \tag{7}$$

$$D = \frac{1}{2} \cdot \left(\nabla \vec{u} + \nabla^T \vec{u} \right) \tag{8}$$

To compare the results for the different setups, the shear rate was normalized by a reference shear rate $\dot{\gamma}_{ref} = U_t / d_b$ to obtain the relative shear rate distribution $\dot{\gamma}'(x,y)$. The results for the Newtonian and non-Newtonian liquid are illustrated in Fig. 4. A higher relative shear rate in the vicinity of the bubble interface is observed for the shear thinning fluid ($\dot{\gamma}'_{\max} = 4.34$) compared to a Newtonian liquid ($\dot{\gamma}'_{\max} = 3.56$). This higher peak value of the shear stress may have an effect on (biological) cells that are aggregated at the bubble interface.

The corresponding dimensionless viscosity field $\mu'(x,y)$ has been obtained by normalizing the computed liquid viscosity field $\mu(x,y)$ with the viscosity $\mu(\dot{\gamma}_{ref})$ at the reference shear rate and is shown in Fig. 5. It clearly indicates that there exists a region in front of the bubble and two separate ones at the rear, where the viscosity is significantly reduced (left figure). Because of the locally higher Re-number in those areas, it can be expected that (especially in the front region of the bubble) the local mass transfer rate will be higher than in Newtonian liquids. That explains the higher overall mass-transfer coefficient that was observed in non-Newtonian liquids at the same Reynolds number.

Another finding is that at higher Re-numbers (Re = 18, right figure), where a closed recirculating wake is formed, a confined region with high viscosity exists that influences the mass transfer from the bubble. This hydrodynamic effect was first observed by Ohta et al. (2005), who investigated bubble flow in a shear-thinning fluid (Carreau-Yasuda model). In our simulations we also observed such a high-viscosity "plug", which has an extent of 1/3rd of the bubble diameter (Fig. 5, right).

Concluding Remarks

Our study shows that the simulation of multiphase flow in non-Newtonian fluids at the micro-scale and the prediction of mass-transfer coefficients for arbitrary fluids are feasible. Even concentration fields can be predicted for moderate Re-numbers and realistic Sc-numbers. Implementation of the rheology of shear-

thinning fluids is straightforward, and the resulting effects can be studied similar to those in Newtonian liquids. Thus, single bubbles and even bubble swarms can be investigated in unprecedented detail. The results of this study are the basis for further research in this area, including:

- *Mass Transfer from bubble swarms in shear thinning fluids.* To connect micro-scale simulations and macro-scale industrial applications, bubble swarms have to be considered.
- *Mass Transfer from bubbles and bubble swarms in viscoelastic fluids.* The effect of viscoelasticity on the mass transfer will be quantified in order to justify the simplifications made in the literature.
- *Biochemical reactions in non-Newtonian fluids.* The model will be enhanced to include chemical reactions in the liquid phase and at the interface between liquid and suspended particles.
- *Combined effects of mass transfer and shear rate distribution in non-Newtonian liquids.* Combined effects of mass transfer rate and shear rate distribution will be considered to find optimal operating conditions.
- *Macro-scale simulation of bioreactors.* The results of the DNS will be used in equipment-size simulations to provide optimization strategies for industrial applications.

Acknowledgement

The authors want to thank Prof. Gretar Tryggvason for providing the front tracking/front capturing code, which was the basis for our modifications. The authors want to acknowledge partial funding of this work through NSF Grant CTS 02098764 and the EU Marie Curie Chair MEXC-CT-2004-006767.

4 Nomenclature

a	Parameter of the Carreau-Yasuda model
c_α	Concentration of species α (kmol/m³)
CFD	Computational Fluid Dynamics
D	Rate of strain tensor (1/s)
D_α	Diffusion coefficient of species α (m²/s)
d_b	volume equivalent bubble diameter (m)
DNS	Direct Numerical Simulation
ds'	Differential element of the bubble contour
ECL-AL	External Circulating Loop Airlift Bioreactors
$\vec{f}$	Body force (gravity; m/s²)
$\vec{F}_\sigma$	Body forces and surface tension (N/m³)
K	Consistency index of the power law model ($Pa \cdot s^n$)
n	Index for time step
n	Flow index of the power law model
$\vec{n}$'	Normal vector to the bubble interface
n_{CY}	Parameter of the Carreau-Yasuda model
p	Pressure (Pa)
r_j	reaction rate of the j-th reaction ($kmol/m^3 \cdot s$)
PDE	Partial differential equation
Pe	Pèclet number ($Pe = d_b \cdot U_t / D_\alpha$)
Re	Bubble Reynolds number ($Re_{newt} = d_b \cdot U_t \cdot \rho_l / \mu_l$, $Re_{power\text{-}law} = d_b^{n} \cdot U_t^{(2-n)} \cdot \rho_l / K$)
Sh	Sherwood number ($Sh = \beta \cdot d_b / D_\alpha$)
Sc	Schmidt number ($Sc = \mu_l / \rho_l \cdot D_\alpha$)
t	Time (s)
$\vec{u}$	Velocity vector (m/s)
$\vec{u}$ *	Intermediate velocity vector (m/s)

U_t Terminal rise velocity (m/s)

$\vec{x}$ Orthogonal coordinates, position vector of a point

$\vec{x}'$ Orthogonal coordinate of the interface

Greek Letters

β Mass transfer coefficient (m/s)

δ Dirac Delta Function

$\dot{\gamma}$ Shear rate (1/s)

$\dot{\gamma}'$ Dimensionless Shear rate

κ' Curvature

λ Parameter of the Carreau-Yasuda model (s)

μ Dynamic viscosity (Pa·s)

μ' Dimensionless dynamic viscosity

μ_∞ Infinite shear rate viscosity of the Carreau-Yasuda model (Pa·s)

μ_0 Zero shear rate viscosity of the Carreau-Yasuda model (Pa·s)

$\nu_{\alpha,j}$ Stoichiometric coefficient of species α in reaction j

ρ Density (kg/m^3)

σ Surface Tension (N/m)

5 References

Al-Masry WA. 1999. Effect of Scale-Up on Average Shear Rates for Aerated non-Newtonian Liquids in External Loop Airlift Reactors. Biotechnol Bioeng 62:494-498 (Communication to the editor).

Bhavaraju SM, Mashelkar RA, Blanch HW. 1978. Bubble motion and mass transfer in non-Newtonian fluids: Part I Single bubble in power law and Bingham fluids. AIChE J 24:1063-1070.

Choi J H, Keum K C, Lee S Y. 2006. Production of recombinant proteins by high cell density culture of *Escherichia coli*. Chem Eng Sci 61:876-885.

Curtis W, Emery A. 1993. Plant cell suspension culture Rheology. Biotechnol Bioeng 42:520-526.

Doran P. 1999. Design of mixing systems for plant cell suspensions in stirred reactors. Biotechnol Prog 16:319-335.

Duddridge JE, Kent CA, Laws JF. 1982. Effect of surface shear stress on the attachment of *Pseudomonas fluorescent* to stainless steel under defined flow conditions. Biotechnol Bioeng 24:153-164.

Gjaltema A, Tijhuis L, van Loosdrecht MCM, Heijnen JJ. 1995. Detachment of biomass from suspended nongrowing spherical biofilms in airlift reactors. Biotechnol Bioeng 46:258-269.

Gjaltema A, van der Marel N, Loosdrecht MCM, Heijnen JJ. 1997. Adhesion and biofilm development on suspended carriers in airlift reactors: Hydrodynamic conditions versus surface characteristics. Biotechnol Bioeng 55:880-889.

Hirose T, Moo-Young M. 1969. Bubble drag and mass transfer in non-Newtonian fluids: creeping flow with power-law fluids. Can J Chem Eng 47:265-267.

Jin B, Lant P, Ge X. 2005. Hydrodynmaics and Mass Transfer Coefficient in Activated Sludge Aerated Stirred Column Reactor: Experimental Analysis and Modeling. Biotechnol Bioeng 91:406-417.

Kawase Y, Hashimoto N. 1996. Gas Hold-Up and Oxygen Transfer in Three-Phase External-Loop Airlift Bioreactors: Non-Newtonian Fermentation Broths. J Chem Tech Biotechnol 65:325-334.

Khinast J. 2001. Impact of 2-D Bubble Dynamics on the Selectivity of Fast Gas-Liquid Reactions. AIChE J 47:2304-2319.

Kieran PM. 1993. An investigation of the hydrodynamic shear susceptibility of suspension cultures of *Morinda citrifolia*. PhD thesis. University College - Dublin (Ireland).

Kieran PM, McLoughlin P, Malone D. 1997. Plant Cell suspension cultures: some engineering considerations. J Biotechnol 59:39-52.

Koynov A, Khinast J, Tryggvason G. 2005. Mass Transfer and Chemical Reactions in Bubble Swarms with Dynamic Interfaces. AIChE J 51:2786-2800.

Lau YL, Liu D. 1993. Effect of flow rate on biofilm accumulation in open channels. Water Res 27:355-360.

Leduy A, Marsan AA, Coupal B. 1974. A study of the rheological properties of a non-Newtonian Fermentation broth. Biotechnol Bioeng 16:61-76.

Leenen EJTM, Martins dos Santos VAP, Grolle KCF, Tramper J, Wijffels RH. 1996. Characteristics of and selection criteria for cell immobilisation in wastewater treatment. Water Res 30:2895-2996.

Li GQ, Qui HW, Zheng ZM, Cai ZL, Yang SZ. 2004. Effect of fluid Rheological properties on mass transfer in a bioreactor. J Chem Tech Biotechnol 65:385-391.

Martins dos Santos VAP, Leenen EJTM, Rippoll MM, van der Sluis C, Vliet T, Tramper J, Wijffels RH. 1997. Relevance of rheological properties of gel beads for their mechanical stability in bioreactors. Biotechnol Bioeng 56:517-529.

Margaritis A, te Bokkel DW, Karamev DG. 1999. Bubble Rise Velocities and Drag Coefficients in Non-Newtonian Polysaccharide Solutions. Biotechnol Bioeng 64:257-266.

Moo-Young M, Hirose T, Ali S. 1970. Rheological effects on liquid phase mass transfer in two phase dispersions: results for creeping flow, Proc 5th Int Cong Rheol, Kyoto 233.

Ohta M, Iwasaki E, Obata E, Yoshida Y. 2005. Dynamic processes in a deformed drop rising through shear-thinning fluids. J Non-Newtonian Fluid Mech 132:100-107.

Rodriguez-Monroy M, Galindo E. 1999. Broth Rheology, growth and metabolite production of *Beta vulgaris* suspension culture: a comparative study between cultures grown in shake flasks and in a stirred tank. Enzyme Microb Technol 24:687-693.

Rodriguez-Monroy M, Galindo E. 2000. Production of arabinogalactanproteins in *Beta vulgaris* cell suspension cultures: a response to hydrodynamic stress. In: Notthnagel E, Basic A, Clarke A; Editors. Cell and Developmental Biology of Arabinogalactan-Proteins, New York: Kluwer Academic Publishers. p 290-292.

Sánchez MJ, Jiménez-Aparicio A, López GG, Tapia GT, Rodríguez-Monroy M. 2002. Broth rheology of Beta vulgaris cultures growing in an air lift bioreactor. Biochem Eng J 12:37-41.

Staniforth A, Côté J. 1991. Semi-Lagrangian Integration Schemes for Atmospheric Models – A review. Mon Weather Rev 119: 2006-2223.

Tryggvason G, Bunner B, Esmaeeli A, Juric D, Al-Rawahi N, Tauber W, Han J, Nas S, Jan Y-J. 2001. A Front-Tracking Method for the Computations of Multiphase Flow. J Comput Phys 169:708-759.

6 List of Figures

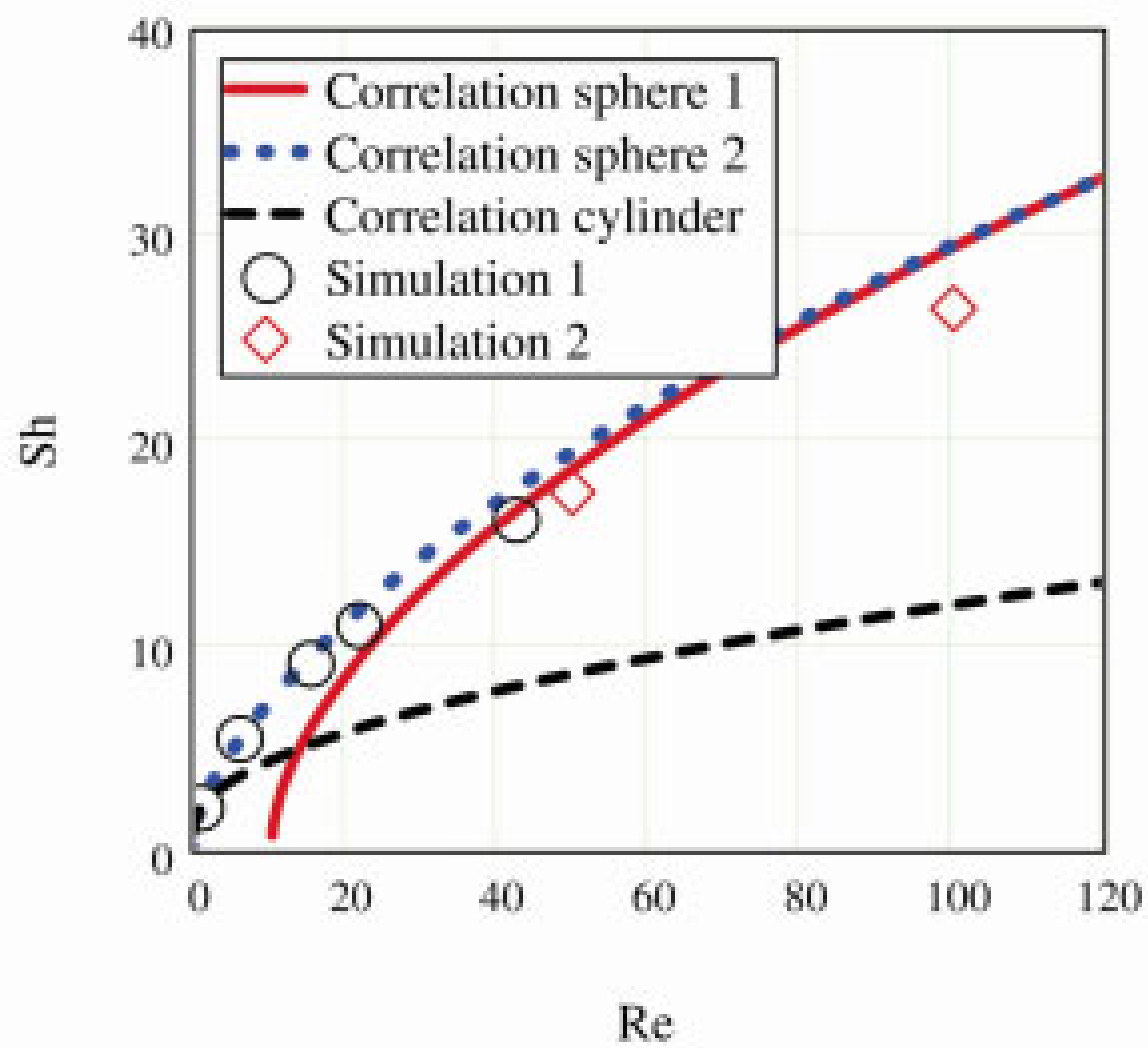
Correlation sphere 1
Correlation sphere 2
Correlation cylinder
Simulation 1
Simulation 2
Sh
Re
0
10
20
30
40
0
20
40
60
80
100
120

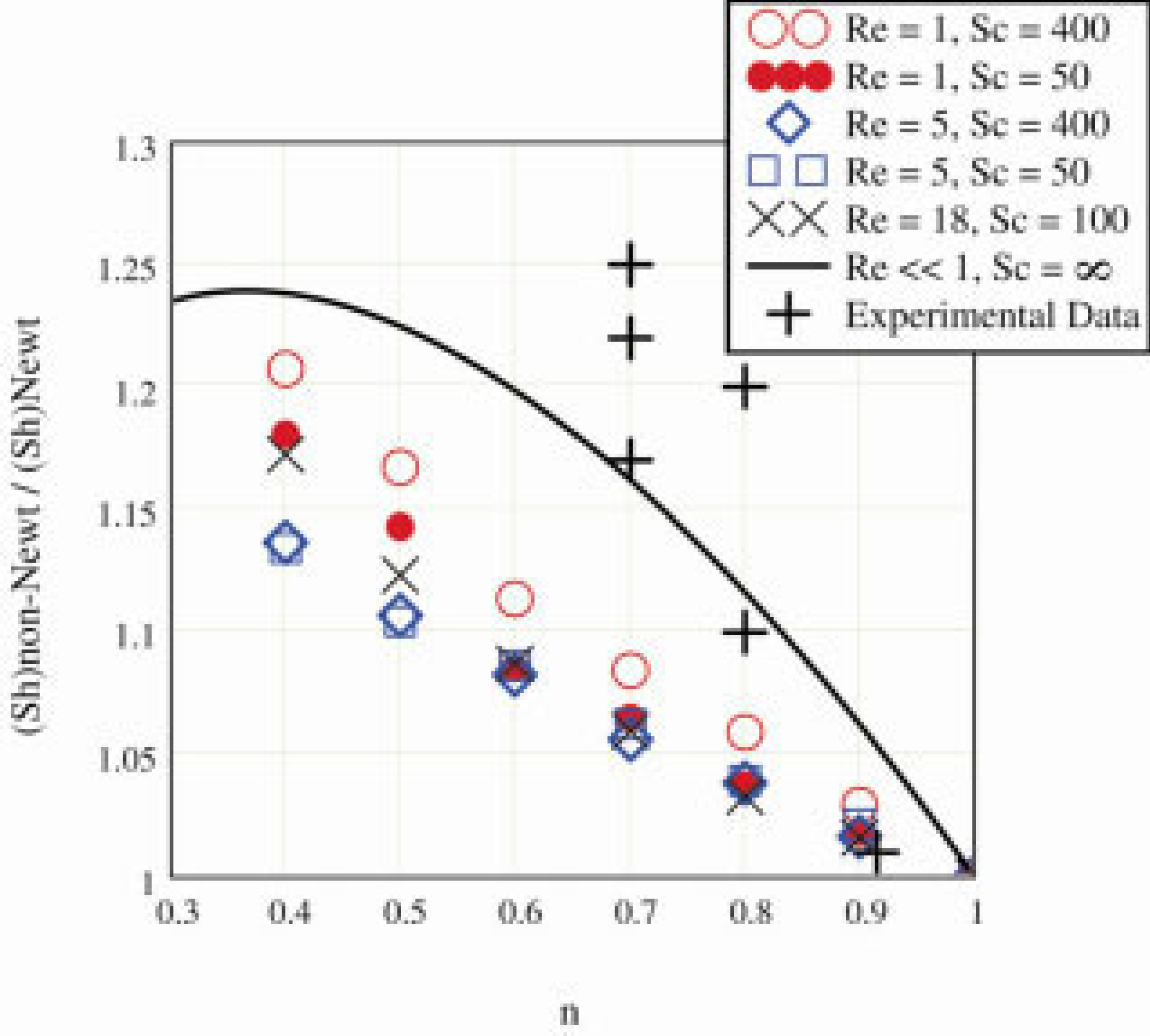
Re = 1, Sc = 400
Re = 1, Sc = 50
Re = 5, Sc = 400
Re = 5, Sc = 50
Re = 18, Sc = 100
Re << 1, Sc = ∞
Experimental Data
(Sh)non-Newt / (Sh)Newt
n
1.3
1.25
1.2
1.15
1.1
1.05
1
0.3
0.4
0.5
0.6
0.7
0.8
0.9
1

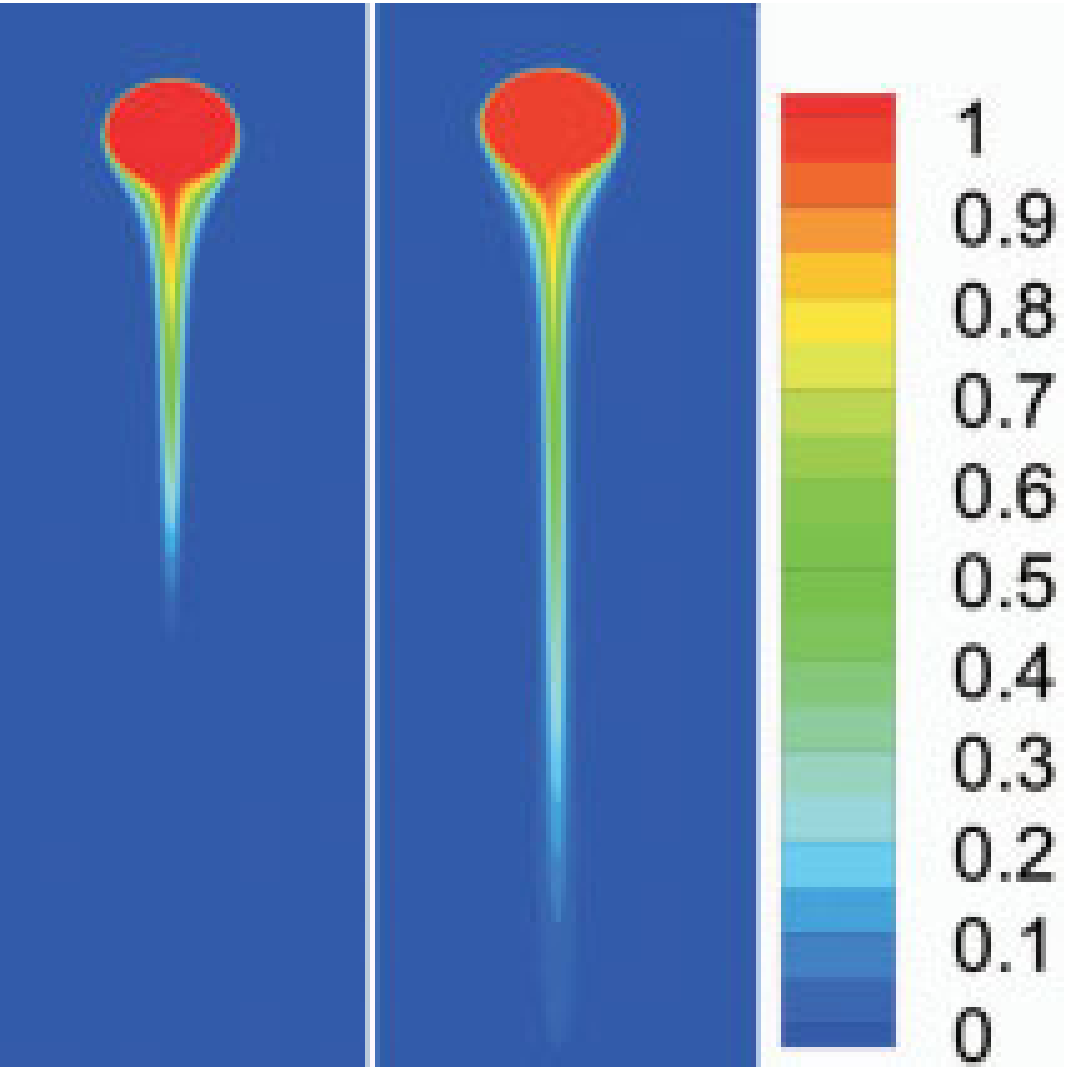
1
0.9
0.8
0.7
0.6
0.5
0.4
0.3
0.2
0.1
0

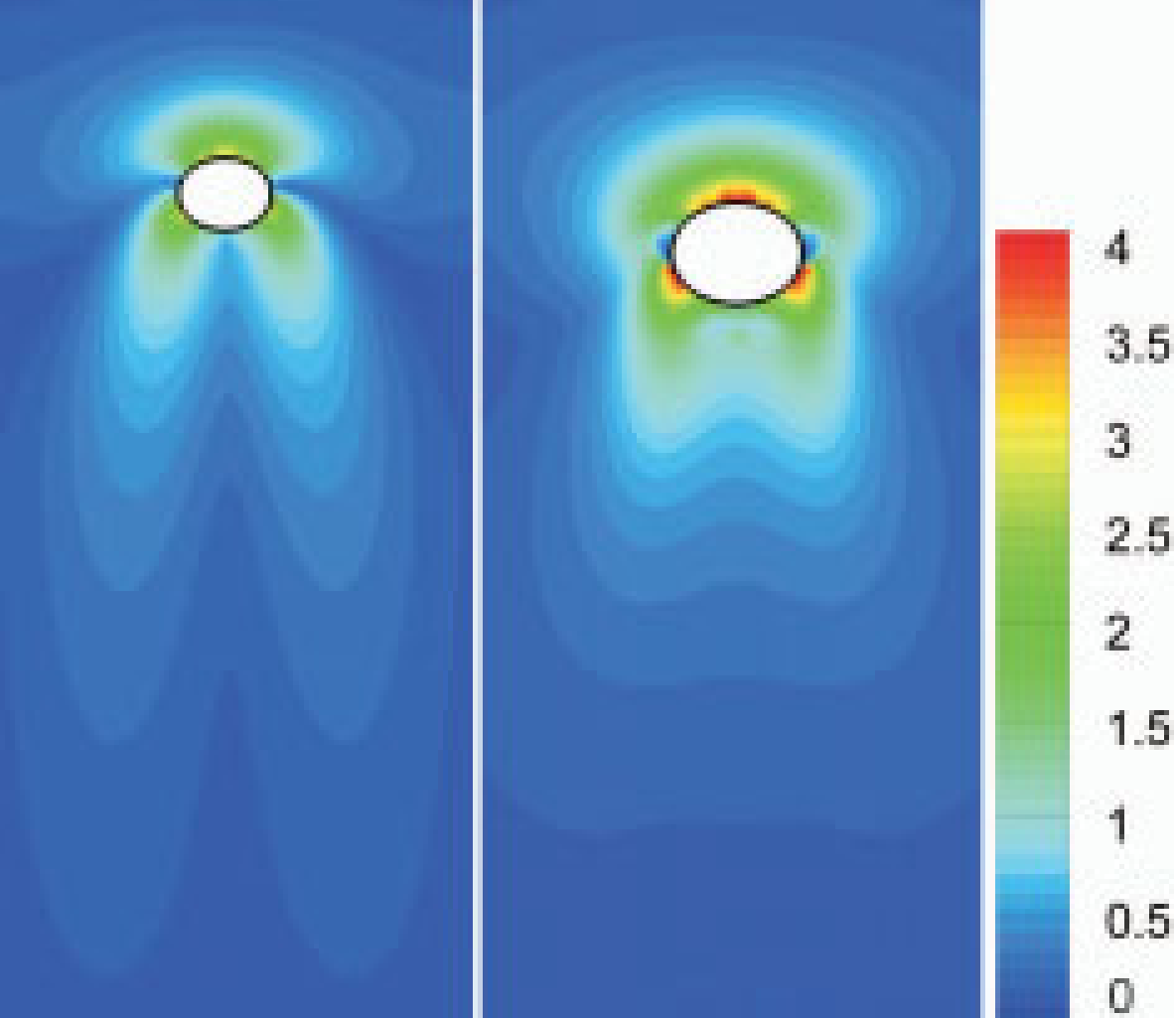
4
3.5
3
2.5
2
1.5
1
0.5
0

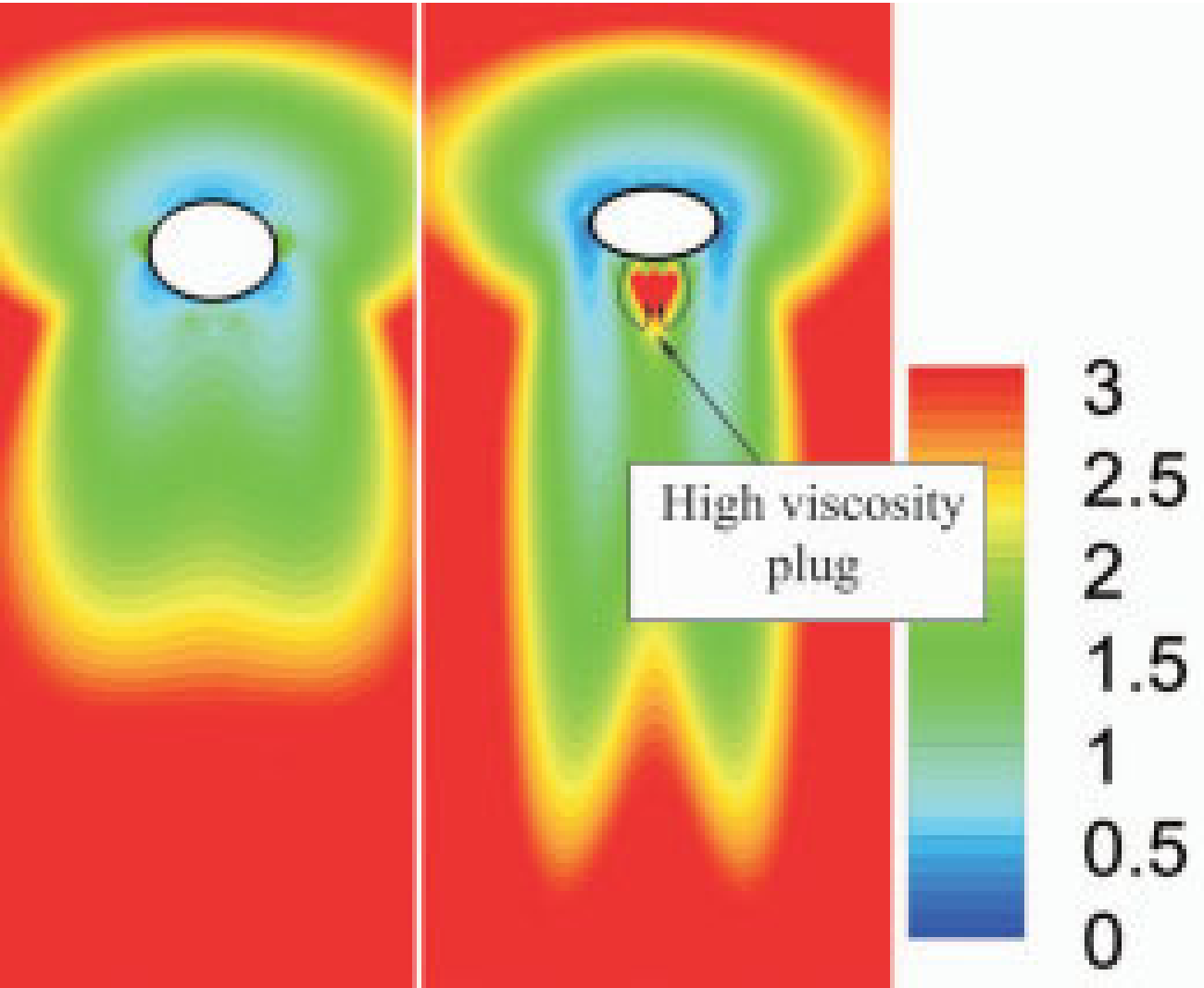
High viscosity plug
3
2.5
2
1.5
1
0.5
0